Predicting modes of operation in quantum dot mode-locked lasers using a delay differential equation model

Jaurigue, Lina, Grillot, Frédéric, Schöll, Eckehard, Lüdge, Kathy

Lina Jaurigue, Frédéric Grillot, Eckehard Schöll, Kathy Lüdge, "Predicting modes of operation in quantum dot mode-locked lasers using a delay differential equation model," Proc. SPIE 9134, Semiconductor Lasers and Laser Dynamics VI, 91342K (2 May 2014); doi: 10.1117/12.2066107

SPIE.

Event: SPIE Photonics Europe, 2014, Brussels, Belgium

Predicting modes of operation in quantum dot mode-locked lasers using a delay differential equation model

Lina Jaurigue[a], Frédéric Grillot[b], Eckehard Schöll[a] and Kathy Lüdge[a]

[a]Institut für Theoretische Physik, Sekr. EW 7-1, Technische Universität Berlin, Hardenbergstr. 36, 10623 Berlin, Germany;
[b]Télécom Paristech, Ecole Nationale Supérieure des Télécommunications, CNRS LTCI, 75634 Paris Cedex 13, France

ABSTRACT

Semiconductor passively mode-locked lasers are of broad interest due to their potential applications as sources of ultra-short, high frequency light pulses. In spite of the complex dynamics of such devices, a relatively simple delay differential equation model can reproduce the manifold modes of operation experimentally observed. Using such a model we investigate the modes of operation of passively mode-locked lasers. We calculate key model parameters from experimentally measured quantities and thus are able to reproduce experimentally observed features, such as the onset of fundamental mode-locking, pulse width and repetition rate. Despite the simplicity of the gain model used within our approach, nano-structured lasers, such as quantum-dot lasers, can be effectively described. This enables us to make predictions about device behavior in dependence of operational parameters and allows for device optimization.

Keywords: passive mode-locking, quantum dot laser, nonlinear dynamics

1. INTRODUCTION

Passively mode-locked (ML) lasers are of broad interest due to their potential applications as sources of ultra-short, high frequency light pulses. They have been the subject to extensive research both theoretically and experimentally.[1–6] In recent years this is particularly true of quantum-dot (QD) semiconductor mode-locked lasers, which are of particular interest due to their favorable properties, such as low threshold currents, low line-width enhancement factors, broad gain spectrum and fast carrier dynamics.[1]

Several theoretical approaches have been developed to study passively mode-locked lasers.[2,7–9] Of these approaches the delay differential equation (DDE) model developed by Vladimirov and Turaev has been widely used in recent years.[10–13] This model assumes a unidirectional ring cavity, comprised of a gain section, an absorber section and a spectral filtering element. It describes the laser dynamics through a delay differential equation for the slowly varying electric field amplitude, coupled to two ordinary differential equations determining the carrier dynamics in the gain and absorber sections. The advantage of this model, for example, compared with a finite-differential traveling wave model, is the greatly reduced computational cost.[3] The DDE model in its original form does not include details of the carrier exchange processes between the QD levels and quantum well reservoirs of QD semiconductor lasers. The model has been extended to include such process,[3,14,15] however this increases the size of the system of equations by at least two and greatly increases the dimensionality of the parameter space. The question we wish to answer in this paper is whether this added complexity is needed to simulate and make predictions about the dynamics of QD semiconductor ML lasers (QDMLL). We do this by using the DDE model in its original form to quantitatively reproduce the experimental results of a QDMLL and investigate the dependence of the ML solution on key parameters.

In this study we model the QDMLL used in the experiments presented in Ref. 16 and Ref. 12. The laser used has a linear cavity of total length 8mm, of which 7mm are the gain section and 1mm is the absorber section. The pulses produced had a repetition frequency of 4.96 GHz with a pulse width of 5.12 ps.[12] We improve the

Further author information: (Send correspondence to L. Jaurigue)
L. Jaurigue: E-mail: linajaurigue@mailbox.tu-berlin.de, Telephone: +49 (0) 30 314 22088

Semiconductor Lasers and Laser Dynamics VI, edited by Krassimir Panajotov, Marc Sciamanna, Angel Valle, Rainer Michalzik, Proc. of SPIE Vol. 9134, 91342K · © 2014 SPIE
CCC code: 0277-786X/14/$18 · doi: 10.1117/12.2066107

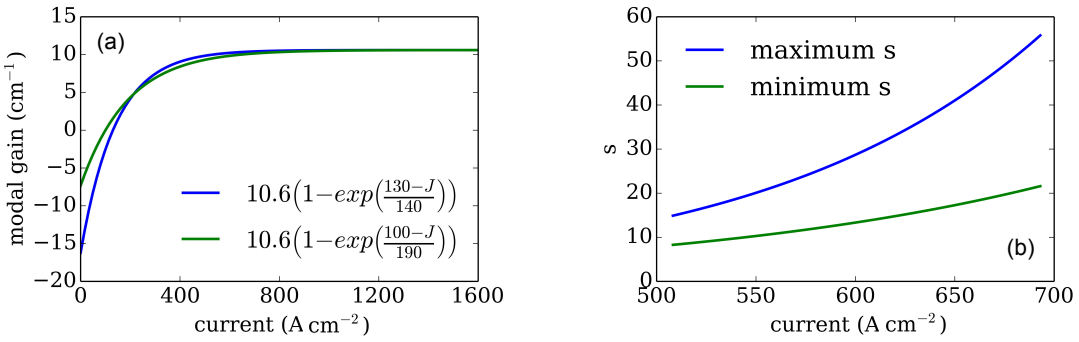

Figure 1. Fits to the modal gain measurements presented in Ref. 16. These fits are used to obtain upper and lower bounds for the ratio of the differential gain in the absorber and gain sections, s, shown in the right panel.

approach to simulate QDMLLs, using the DDE model, that was made in Ref. 12. We use some of the methods of calculating parameter values from experimental measurements that were used in this work.

The paper is organised into three subsequent sections. In Section 2 the DDEs and the methods for calculating the DDE parameter values from experimental measurements are introduced. In Section 3 the results are presented and discussed and finally, in Section 4 the conclusions are presented.

2. MODEL AND CALCULATION OF PARAMETERS

2.1 DDE Model

The set of DDEs derived by Vladimirov and Turaev[9] is given by

$$\frac{dA(\tau)}{d\tau} = \gamma\sqrt{\kappa}e^{\left[\frac{1}{2}((1-i\alpha_g)G(\tau-T)-(1-i\alpha_q)Q(\tau-T))\right]}A(\tau-T)-\gamma A(\tau), \tag{1}$$

$$\frac{dG(\tau)}{d\tau} = g_0-\Gamma G(\tau)-e^{-Q(\tau)}\left(e^{G(\tau)}-1\right)|A(\tau)|^2 \tag{2}$$

and

$$\frac{dQ(\tau)}{d\tau} = q_0-Q(\tau)-s\left(1-e^{-Q(\tau)}\right)|A(\tau)|^2. \tag{3}$$

These equations describe a ring cavity laser with a gain section, an absorber section and a spectral filter. The three dynamical variables are the dimensionless electric field amplitude A, saturable gain G and saturable loss Q. G and Q describe the gain and resonant losses for one roundtrip in the laser cavity.

In Eqs. (1)-(3) the non-resonant linear intensity losses per roundtrip are described by κ. The gain spectrum is taking into an account by a Lorentzian-shaped spectral filter with full-width at half maximum γ. The parameters α_g and α_q are the linewidth-enhancement factors (α-factors) in the gain and absorber sections, respectively. The unsaturated gain and losses, introduced by pumping the gain section and applying a reverse bias to the absorber section, are given by g_0 and q_0, respectively. The parameter Γ is the ratio of the relaxation time in the absorber and gain sections (τ_q/τ_g), and s is the ratio of the differential gain in the absorber and gain sections ($g_q\Gamma_q/g_g\Gamma_g$).

Equations 1-3 are formulated in a frame of reference co-moving with the pulse propagating in the cavity, with retarded time $\tau = \frac{1}{\tau_q}\left(t-\frac{z}{v}\right)$ in units of the absorber relaxation time τ_q. The delay time $T = \frac{1}{\tau_q}\frac{L}{v}$ is the cold cavity roundtrip time (L is the ring cavity length).

2.2 Calculation of model parameters from experimental results

Adding together the total intensity losses and gain for one roundtrip one obtains the following threshold condition for lasing:[16]

$$\left(g_{\mathrm{mod}}\left(J\right)-\alpha_i\right)2L_g-\left(a_0+\alpha_i\right)2L_q-\alpha_m 2\left(L_q+L_g\right)=0, \tag{4}$$

with

$$\alpha_m=\frac{1}{2\left(L_g+L_q\right)}\ln\left(\frac{1}{R_1R_2}\right). \tag{5}$$

Here L_g and L_q are the lengths of the gain and absorber sections, respectively, $g_{\mathrm{mod}}\left(J\right)$ is the current dependent modal gain, a_0 is the unsaturated absorption, α_i is the internal loss, α_m is the mirror loss and R_1, R_2 are the facet intensity reflectivities. From Eq. (1) above the following threshold condition for lasing can be obtained:

$$\kappa e^{(G-Q)}=1. \tag{6}$$

This is obtained by assuming steady state lasing, and corresponds to the total intensity losses and gain for one roundtrip. The non-linear intensity losses per roundtrip are defined as

$$\kappa=R_1R_2e^{-2\alpha_i\left(L_g+L_q\right)}. \tag{7}$$

Using this definition for κ and and the two threshold conditions (Eqs. 4 and 6) one obtains

$$G_{th}=g_{\mathrm{mod}}\left(J\right)2L_g \tag{8}$$

and

$$Q_{th}=a_0 2L_q \tag{9}$$

where G_{th} and Q_{th} indicate the gain G and saturable loss Q at threshold, respectively. The threshold conditions for Eqs. (2) and (3) are $g_0^{th}=\Gamma G_{th}$ and $q_0^{th}=Q_{th}$, respectively. Therefore, in terms of experimentally measurable quantities we have

$$g_0^{th}=\Gamma g_{\mathrm{mod}}\left(J\right)2L_g \tag{10}$$

and

$$q_0^{th}=a_0 2L_q. \tag{11}$$

Mode-locking occurs above the threshold current, and as g_0 is current dependent its value will depend on the current at which mode-locking is achieved. However, the unsaturated absorption q_0 depends only on the reverse bias applied to the absorber section and is not influenced by the pump current injected into the gain section. It is therefore given by the threshold condition, $q_0=a_0 2L_q$. Mode-locking is achieved at 1.1-1.5 times the lasing threshold current, J^{th}.[5,12,17] The unsaturated gain is proportional to $\left[g_g\Gamma_g\right]_J\left(J-J^{tr}\right)$, where J^{tr} is the transparency current of the linearised gain and $\left[g_g\Gamma_g\right]_J$ is the slope of the gain function linearised at J. The range of possible values for g_0 is given by

$$g_0=\frac{\left[g_g\Gamma_g\right]_{xJ^{th}}\left(xJ^{th}-J^{tr}\right)}{\left[g_g\Gamma_g\right]_{J^{th}}\left(J^{th}-J^{tr}\right)}g_0^{th}, \tag{12}$$

with x=1.1-1.5. Here $\left[g_g\Gamma_g\right]_X$ is the linearised gain at current X.

The ratio of the differential gain in the absorber and gain sections, s, can be calculated from the experimentally measured modal gain using[12]

$$s\equiv\frac{g_q\Gamma_q}{\left[g_g\Gamma_g\right]_J}=\frac{\left[\partial g_{\mathrm{mod}}\left(J\right)/\partial J\right]_{g_{\mathrm{mod}}{}^{(J)=0}}}{\left[\partial g_{\mathrm{mod}}\left(J\right)/\partial J\right]}, \tag{13}$$

The function describing the current dependence of the modal gain is obtained by fitting experimental data, as done in Ref. 16. In this study the authors have fit a function of the form

$$g_{\mathrm{mod}}\left(J\right)=g_{\mathrm{max}}\left[1-\exp\left(\frac{J^{tr}-J}{\epsilon}\right)\right] \tag{14}$$

to the experimental data. To obtain upper and lower bounds for the value of s we fit these modal gain measurements as shown in fig. 1 (a). The green curve fits the data well for currents much larger than the transparency current, however, near transparency the slope of this function is too shallow, leading to the maximum absorption being much smaller than the maximum gain. The blue curve describes the gain at low currents more accurately.[18] In fig. 1 (b) the resulting minimum and maximum s values are plotted.

Finally, the spectral filter coefficient γ can be obtained from the width of the optical spectrum.

Using the experimental measurements given in Ref. 16 and Ref. 12 we calculate the DDE model parameters as described above. In Ref. 16 and Ref. 12 the recovery times of the absorber and gain sections were not measured. We must therefore estimate these from measurements carried out on similar devices.[19,20] The experimentally measured quantities and calculated DDE model parameter values are summarized in Table 1. Based on the data available we have a range of possible values κ, Γ and s, but we do not have any experimental indications for the values of the amplitude-phase coupling in the absorber sections. In the subsequent section we therefore first investigate the influence of the these parameters on the output of a the simulated ML laser.

Table 1. Physical parameters (left column) used to calculate the simulation parameters (right column).

Physical Parameter	Value		DDE Parameter	Value
L_g	1 mm		q_0	5.74
L_q	7 mm		T	5.74
α_i	1.6-3.3 cm^{-1}		κ	0.0015-0.02
R_1R_2	0.30		γ	39.15
$g_{\mathrm{mod}}(J^{th}$=462 $\mathrm{Acm}^{-2})$	9.2 cm^{-1}		Γ	0.117-0.35
a_0	28.7 cm^{-1}		s	7-55
τ_q	35 ps[19]		α_g	varied
τ_g	100-300 ps[20]		α_q	varied

3. RESULTS AND DISCUSSION

In this section the dependence, of the output of the simulated ML laser, on key model parameter is investigated. We then use these results to find model parameters, within the range of experimentally calculated values, that reproduce the output of the QDMLL studied in Ref. 16 and Ref. 12.

For high non-resonant losses, κ, we do not find ML within the appropriate DDE parameter range. For $\kappa = 0.0015$ the ratio of the differential gain in the absorber and gain sections, s, has to be larger than 120 for ML to occur, which is much larger than the values we get from the measured modal gain curves (see fig. 1 (b)). In the subsequent simulations we therefore use $\kappa = 0.02$, the lower loss limit of the experimentally determined κ range.

In fig. 2 the influence of the ratio of the differential gain in the absorber and gain sections, s, the unsaturated gain, g_0, and the relaxation time in the gain section, τ_g, are shown. White regions indicate continuous wave (CW) emission, orange regions indicate fundamental or harmonic ML (ML) and blue regions indicate quasi-periodic ML or deformed pulses ($other$). The laser is off in the gray regions (off). The threshold unsaturated gain, g_0^{th}, depends on τ_g (Eq. 10), accordingly the laser turns on at increasing values of g_0 in subplots (a) to (d), which correspond to $\tau_g = 300ps$, $\tau_g = 200ps$, $\tau_g = 100ps$ and $\tau_g = 50ps$, respectively. With decreasing τ_g we also find that larger s values are needed to achieve ML. Furthermore, the onset of ML is shifted further away from the lasing threshold to larger values of g_0. However, in all four cases (subplots (a)-(d)) the onset of FML occurs within 1.1-1.5 times threshold, which is consistent with the experimental results.[12,16]

The areas of ML are more prevalent for smaller values of the unsaturated gain. For fixed s and increasing g_0 the system goes through a series of bifurcations, exhibiting harmonic and quasi-periodic ML and eventually

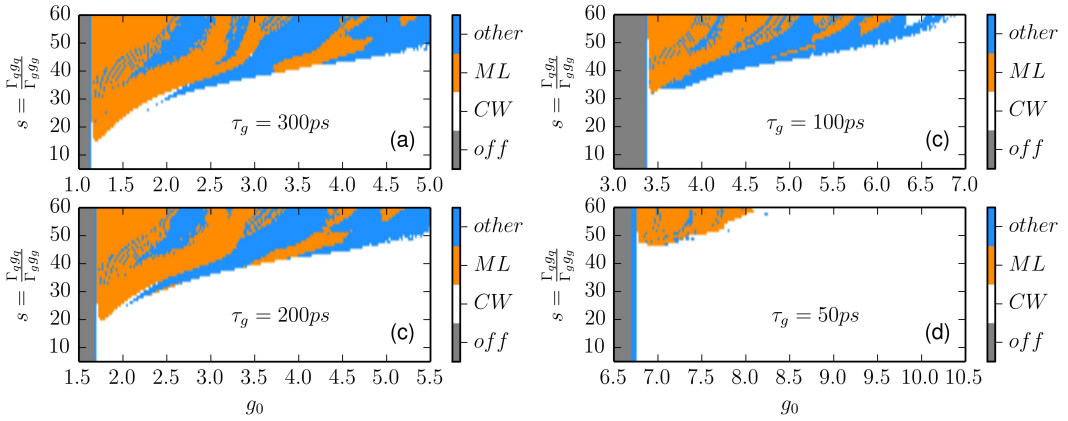

Figure 2. Bifurcation diagrams showing the mode of operation of the simulated ML laser in dependence of the ratio of the differential gain in the absorber and gain sections, s, and the unsaturated gain, g_0, for $\tau_g = 300ps$ (a), $\tau_g = 200ps$ (b), $\tau_g = 100ps$ (b) and $\tau_g = 50ps$ (d). Gray regions (off) indicate that the laser is off, white regions (CW) indicate continuous wave emission, orange regions (ML) indicate fundamental or harmonic ML and blue regions ($other$) indicate quasi-periodic ML or deformed pulses. Parameters: $\alpha_g = \alpha_q = 0.5$, $\kappa = 0.02$, remaining parameters as in Table 1.

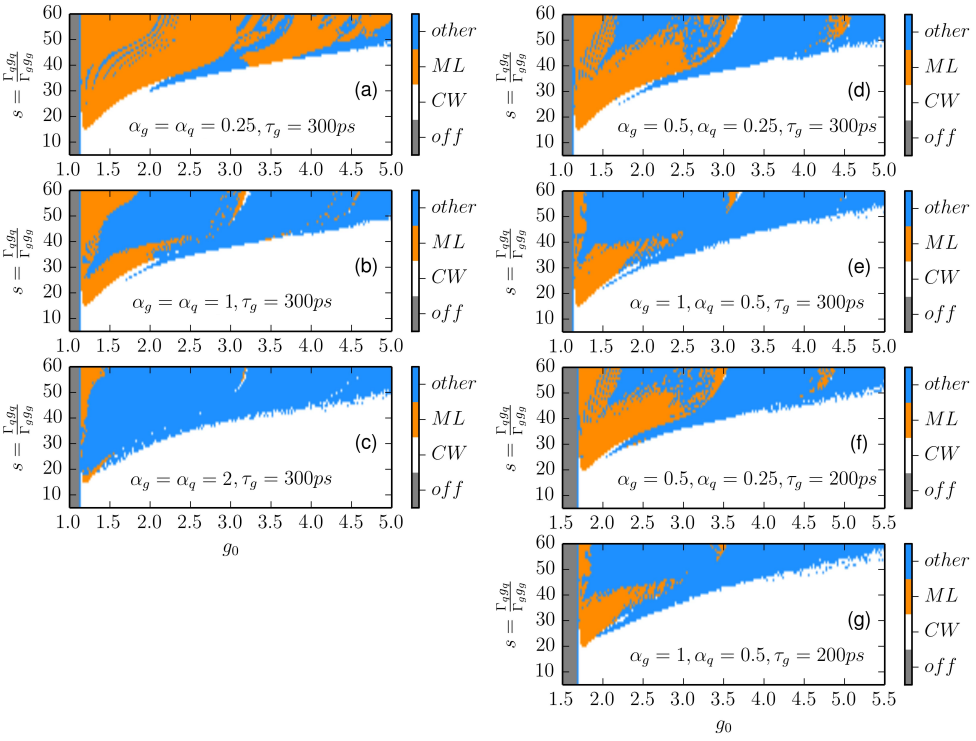

Figure 3. Bifurcation diagrams showing the mode of operation of the simulated ML laser in dependence of the ratio of the differential gain in the absorber and gain sections, s, and the unsaturated gain, g_0, for $\alpha_g = \alpha_q = 0.25$ (a), $\alpha_g = \alpha_q = 1$ (b) and $\alpha_g = \alpha_q = 2$ (c) with $\tau_g = 300ps$, and for $\tau_g = 300ps$ (d,e) and $\tau_g = 200ps$ (f,g) with unequal α-factors in the gain an absorber sections . Gray regions (off) indicate that the laser is off, white regions (CW) indicate continuous wave emission, orange regions (ML) indicate fundamental or harmonic ML and blue regions ($other$) indicate quasi-periodic ML or deformed pulses. Parameters: $\kappa = 0.02$, remaining parameters as in Table 1.

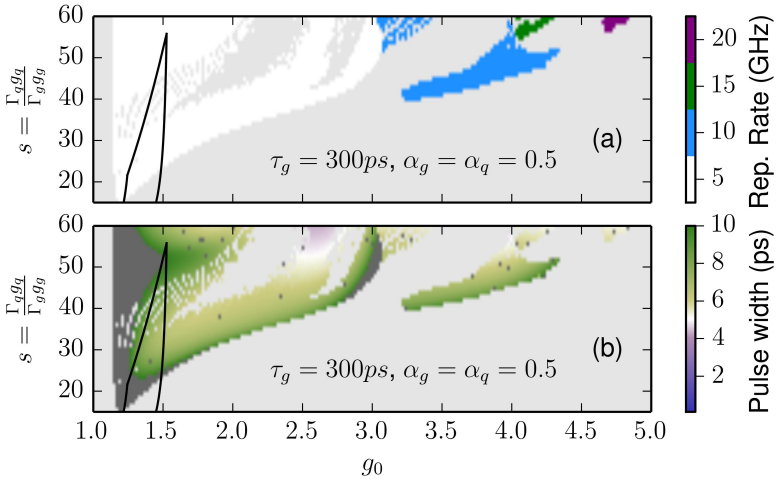

Figure 4. (a) Pulse repetition rate in regions of ML in s-g_0 parameter space. (b) Pulse full width at half maximum in regions of fundamental ML in s-g_0 parameter space. In the light gray regions there is no ML. The dark gray regions in the bottom panel indicate pulse widths larger than 10 ps. The black lines in the bottom panel indicate the experimentally determined limits for s and g_0. Parameters: $\alpha_g = \alpha_q = 0.5$, $\tau_g = 300ps$, $\kappa = 0.02$, remaining parameters as in Table 1.

continuous wave emission. This is consistent with previous theoretical studies on the dependence of the laser output on g_0.[9,21]

In fig. 2 the amplitude-phase coupling in the gain and absorber section was chosen to be 0.5. In figure 3 we show similar bifurcation diagrams for different α-factors. In fig. 3 (a)-(c) $\tau_g = 300ps$ and the α-factors in the gain and absorber sections are chosen to be equal. Here we see that with increasing α-factors the regions of fundamental ML decrease. With unequal α-factors in the gain and absorber sections we also observed less fundamental ML in the s-g_0 parameter space (fig. 3 (d)-(g)). The amplitude-phase coupling influences the pulse shape, for larger or unequal α-factors the pulses can be deformed, have multiple peaks or the peak height can be modulated over multiple cavity round trips. These effects cause the reduction in the regions of ML. Comparing fig. 2 (a) with fig. 3 (d), and fig. 3 (a) with fig. 3 (d), we can see that changing only α_q has less of an effect on the ML regions than changing only α_g. The gain section of the laser is longer than the absorber section, therefore it is expected that the amplitude-phase coupling in the gain section has a greater effect on the dynamics of the laser. The amplitude-phase coupling, however, does not have a great influence on the transition to continuous wave emission (transition from colored to white region in figures 2 and 3).

To find parameter values, within the experimentally calculated ranges, that reproduce the experimentally observed frequency and pulse width, we calculate these quantities for the observed regions of fundamental ML (figures 4 and 5). Panel (a) of fig. 4 shows the pulse repetition rate as a function of s and g_0. Here regions of fundamental and harmonic ML are clearly distinguishable. Up to about $g_0 = 3.0$ fundamental ML with a frequency of about 5 GHz is simulated. Above $g_0 = 3.0$ harmonic ML, up to fourth order, can be observed. Within the region of fundamental ML (white region in fig. 4 (a)) there is very little variation in the repetition rate in s-g_0 space ($f_{\text{rep}} = 4.95 \pm 0.05$ GHz). In fig. 4 (b) the corresponding pulse widths are plotted. Regions in white indicate a pulse with of 5 ps, corresponding to the experimentally measured pulse width. The black curves depicted in this plot enclose the experimentally determined range for s and g_0. The simulation results in fig. 4 are for $\tau_g = 300ps$ and $\alpha_g = \alpha_q = 0.5$, for these parameter values we can not simulate a pulse width of 5.12 ps in the appropriate s and g_0 ranges.

In fig. 5 pulse repetition rates and pulse widths are plotted for various τ_g and amplitude-phase couplings. In (a) and (b) $\alpha_g = 0.5$, $\alpha_q = 0.25$ and $\tau_g = 300ps$. Compared with fig. 4 ($\alpha_g = \alpha_q = 0.5$ and $\tau_g = 300ps$) the regions with pulse widths of about 5 ps are shifted to lower s values. However, the simulated pulse widths within the experimentally determined s-g_0 region are all larger than 5.12 ps. Varying the amplitude-phase coupling, we were not able to simulate the experimentally observed pulse widths within the experimentally determined s-g_0

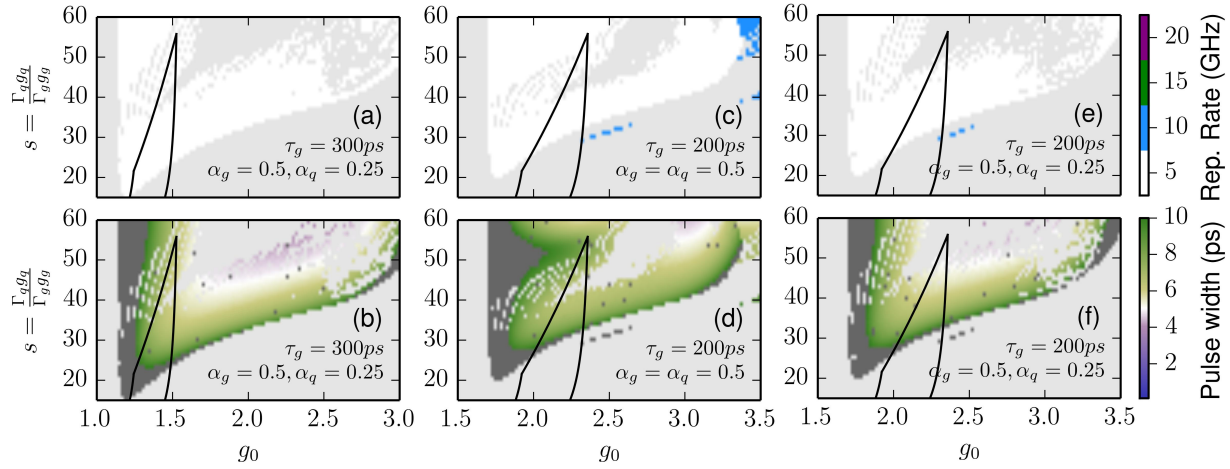

Figure 5. Pulse repetition rate in regions of ML in s-g_0 parameter space for $\alpha_g = 0.5$, $\alpha_q = 0.25$, $\tau_g = 300ps$ (a), $\alpha_g = \alpha_q = 0.5$, $\tau_g = 200ps$ (c) and $\alpha_q = 0.25$, $\tau_g = 300ps$, $\tau_g = 200ps$ (e). Pulse full width at half maximum in regions of fundamental ML in s-g_0 parameter space for $\alpha_g = 0.5$, $\alpha_q = 0.25$, $\tau_g = 300ps$ (b), $\alpha_g = \alpha_q = 0.5$, $\tau_g = 200ps$ (d) and $\alpha_q = 0.25$, $\tau_g = 300ps$, $\tau_g = 200ps$ (f). In the light gray regions there is no ML. The dark gray regions in the bottom panel indicate pulse widths larger than 10 ps. The black lines in the bottom panel indicate the experimentally determined range for s in the g_0 range $1.0g_0^{th}$-$2.4g_0^{th}$. Parameters: $\kappa = 0.02$, remaining parameters as in Table 1.

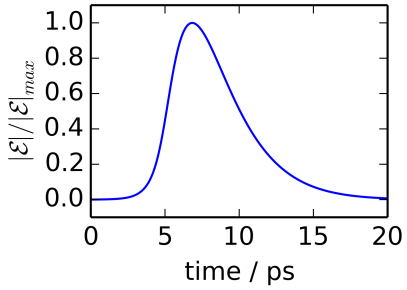

Figure 6. Time trace of electric field intensity. Parameters: $\tau_g = 200ps$, $\kappa = 0.02$, $\alpha_g = 0.5$, $\alpha_q = 0.25$, $g_0 = 2.34$, $s = 47$, remaining parameters as in Table 1.

region for $\tau_g = 300ps$. In (c)-(f) of fig. 5, τ_g is chosen to be 200 ps. For equal amplitude-phase coupling in the gain and absorber sections we can not simulate the experimentally observed pulse widths within the appropriate s, g_0 range (fig. 5 (c) and (d) show the simulation results for $\alpha_g = \alpha_q = 0.5$). However, for $\alpha_g = 0.5$, $\alpha_q = 0.25$ we are able to closely simulate the experimental results. For $s = 47$ and $g_0 = 2.34$ the simulated repetition rate and pulse width are 4.96 GHz and 5.19 ps, respectively. The simulation results in dependence of the amplitude-phase coupling allow us to give bounds to α_g and α_q. We find the $\alpha_g < 1$ and $\alpha_q < 0.5$.

In Ref. 12 frequency-resolved optical gating (FROG) measurements were also performed. Time traces of these measurements showed asymmetric pulses with a shallow leading edge and steep trailing edge. In fig. 6 a time trace of a simulated pulse for $s = 47$ and $g_0 = 2.34$ is shown. The pulse shape is in qualitative agreement with the measured pulse shape from Ref. 12.

As we are able to reproduce the pulse repetition rate, pulse width and pulse shape using the DDE model and the method of calculating the model parameters from experimentally measured quantities that is given in Section 2.2, we believe this model also has predictive capabilities. Given the necessary input parameters this model should be able to predict the possible pulse width and dependence on the pump current.

4. CONCLUSIONS

Using the relatively simple DDE model developed by Vladimirov and Turaev, which does not include details of the quantum dot structure, we are able to reproduce the pulse repetition rate, pulse width, and pulse shape of a quantum-dot passively mode-locked laser. This is done using realistic parameters values, calculated from experimentally measured quantities. Furthermore, we are able to simulate key features in dependence of the pump current. Firstly, the onset of mode-locking is shown to occur shortly after the lasing threshold, as observed in experiments. Secondly, for large values of the unsaturated gain, which depends on the pump current, continuous wave emission is observed.

We have investigated the model dependence on the amplitude-phase coupling and have shown that given experimental details concerning the pulse properties we can give upper bounds for α_g and α_q, i.e. $\alpha_g < 1$ and $\alpha_q < 0.5$ for the simulated QDMLL. The amplitude-phase coupling has a significant effect on the laser dynamics within the ML regime, however for the borders of the continuous wave regime it has little effect.

ACKNOWLEDGMENTS

We thank B. Lingnau and C. Otto for fruitful discussion and acknowledge support from the GRK 1558 funded by the DFG. KL and FG acknowledge support from the DAAD for the PPP project with France.

REFERENCES

1. M. G. Thompson, A. R. Rae, M. Xia, R. V. Penty, and I. H. White, "InGaAs quantum-dot mode-locked laser diodes," *IEEE J. Quantum Electron.* **15**(3), pp. 661–672, 2009.
2. M. Rossetti, P. Bardella, and I. Montrosset, "Time-domain travelling-wave model for quantum dot passively mode-locked lasers," *IEEE J. Quantum Electron.* **47**(2), p. 139, 2011.
3. M. Rossetti, P. Bardella, and I. Montrosset, "Modeling passive mode-locking in quantum dot lasers: A comparison between a finite- difference traveling-wave model and a delayed differential equation approach," *IEEE J. Quantum Electron.* **47**(5), p. 569, 2011.
4. M. Rossetti, X. Tianhong, P. Bardella, and I. Montrosset, "Impact of gain saturation on passive mode locking regimes in quantum dot lasers with straight and tapered waveguides," *IEEE J. Quantum Electron.* **47**(11), p. 1404, 2011.
5. L. Drzewietzki, S. Breuer, and W. Elsäßer, "Timing phase noise reduction of modelocked quantum-dot lasers by time-delayed optoelectronic feedback," *Electron. Lett.* **49**(8), 2013.
6. S. Breuer, W. Elsäßer, J. G. McInerney, K. Yvind, J. Pozo, E. A. J. M. Bente, M. Yousefi, A. Villafranca, N. Vogiatzis, and J. Rorison, "Investigations of repetition rate stability of a mode-locked quantum dot semiconductor laser in an auxiliary optical fiber cavity," *IEEE J. Quantum Electron.* **46**(2), p. 150, 2010.
7. G. New, "Pulse evolution in mode-locked quasi-continuous lasers," *IEEE J. Quantum Electron.* **10**(2), p. 115, 1974.
8. H. A. Haus, "Theory of mode locking with a slow saturable absorber," *IEEE J. Quantum Electron.* **11**(9), p. 736, 1975.
9. A. G. Vladimirov and D. Turaev, "Model for passive mode locking in semiconductor lasers," *Phys. Rev. A* **72**(3), p. 033808, 2005.
10. K. Lüdge, *Nonlinear Laser Dynamics - From Quantum Dots to Cryptography*, Wiley-VCH, Weinheim, 2012.
11. C. Otto, K. Lüdge, A. G. Vladimirov, M. Wolfrum, and E. Schöll, "Delay induced dynamics and jitter reduction of passively mode-locked semiconductor laser subject to optical feedback," *New J. Phys.* **14**, p. 113033, 2012.
12. R. Raghunathan, M. T. Crowley, F. Grillot, Y. Li, J. K. Mee, V. Kovanis, and L. F. Lester, "Pulse characterization of passively mode-locked quantum-dot lasers using a delay differential equation model seeded with measured parameters," *IEEE J. Sel. Top. Quantum Electron.* **19**(4), p. 1100311, 2013.
13. U. Bandelow, M. Radziunas, A. G. Vladimirov, B. Httl, and R. Kaiser, "40GHz mode locked semiconductor lasers: Theory, simulation and experiments," *Optical and Quantum Electronics* **38**, p. 495, 2006.

14. A. G. Vladimirov, U. Bandelow, G. Fiol, D. Arsenijević, M. Kleinert, D. Bimberg, A. Pimenov, and D. Rachinskii, "Dynamical regimes in a monolithic passively mode-locked quantum dot laser," *J. Opt. Soc. Am. B* **27**(10), p. 2102, 2010.
15. C. Simos, H. Simos, C. Mesaritakis, A. Kapsalis, and D. Syvridis, "Pulse and noise properties of a two section passively mode-locked quantum dot laser under long delay feedback," *Opt. Commun.* **313**, pp. 248–255, 2014.
16. M. T. Crowley, D. Murrell, N. Patel, M. Breivik, C.-Y. Lin, Y. Li, B.-O. Fimland, and L. F. Lester, "Analytical modeling of the temperature performance of monolithic passively mode-locked quantum dot lasers," *IEEE J Quantum Electron* **47**(8), pp. 1059–1068, 2011.
17. M. T. Crowley, J. Houlihan, T. Piwonski, I. O'Driscoll, D. P. Williams, E. P. O'Reilly, A. V. Uskov, and G. Huyet, "Refractive index dynamics of inas/gaas quantum dots," *Appl. Phys. Lett.* **103**, p. 021114, 2013.
18. D. R. Matthews, H. D. Summers, P. M. Smowton, and M. Hopkinson, "Experimental investigation of the effect of wetting-layer states on the gainâcurrent characteristic of quantum-dot lasers," *Appl. Phys. Lett.* **81**(26), pp. 4904–4906, 2002.
19. M. A. Cataluna, D. B. Malins, A. Gomez-Iglesias, W. Sibbett, A. Miller, and E. U. Rafailov, "Temperature dependence of electroabsorption dynamics in an inAs quantum-dot saturable absorber at $1.3\mu m$ and its impact on mode-locked quantum-dot lasers," *Appl. Phys. Lett.* **97**(12), p. 121110, 2010.
20. T. Vallaitis, C. Koos, R. Bonk, W. Freude, M. Laemmlin, C. Meuer, D. Bimberg, and J. Leuthold, "Slow and fast dynamics of gain and phase in a quantum dot semiconductor optical amplifier," *Opt. Express* **16**(1), pp. 170–178, 2008.
21. A. G. Vladimirov, D. Turaev, and G. Kozyreff, "Delay differential equations for mode-locked semiconductor lasers," *Opt. Lett.* **29**(11), p. 1221, 2004.